A Novel Consolidation Method to Measure Powder Flow Properties Using a Small Amount of Material

Sara Koynov, Fernando J. Muzzio, and Benjamin J. Glasser
Dept. of Chemical and Biochemical Engineering, Rutgers University, 98 Brett Road, Piscataway, NJ 08854

DOI 10.1002/aic.15321
Published online June 3, 2016 in Wiley Online Library (wileyonlinelibrary.com)

Bulk flow property characterization often requires large powder samples (tens to hundreds of grams). However, many applications have limited sample availability, due to cost, material availability, safety concerns, etc. Therefore, reducing the amount of required material is of interest. A novel compressibility method is introduced using less than 50 mg, for the materials studied here. The effect of particle size and cohesion due to capillary forces are determined using a small-scale compressibility cell mounted on a texture analyzer. It is found that the powder bed consolidation occurred in two regimes, described using the Walker and Heckel equations. The small-scale compressibility method was compared to known behavior at larger scales and validated against the FT4 compressibility test. It was found that bulk behavior could be observed using the small-scale compressibility method. Additional behavior caused by small-scale events, which are averaged out in large-scale measurements, are revealed in the small-scale device introduced here. © 2016 American Institute of Chemical Engineers *AIChE J*, 62: 4193–4200, 2016
Keywords: powder, cohesion, packing, compressibility

Introduction

Powders appear both in nature and industrial processes and it has been estimated that half of all industrial products involve powder processing.[1–6] However, a general theoretical approach based on constitutive equations for describing granular flow and behavior has, to date, not been developed.[7] As a result, prediction of the performance of solids processing operations is difficult and relies on experimentally obtained powder flow characteristics.[8,9] Powder flow characterization has been used in multiple industries to improve the understanding of process unit operations. For example, the catalysis industry has applied powder flow characterization methods to the study of impregnation, drying, mulling, and calcination processes,[10,11] and the pharmaceutical industry has applied them to processes including agitated drying, powder blending, tabletting, and prediction of attrition,[12–18] among many others. In some cases, the characterization method can be optimized for a particular application, such as modifying the measurement cell size.[19,20] The ability to perform powder flow characterization is often limited by the amount of material required for testing, often tens to hundreds of grams of material. There are instances where the material available for testing is limited, due to the cost of the material, availability of the material, safety concerns, etc. Hughes et al. attempted to develop a material sparing bulk density test for use in such situations.[21] Here, the smallest sample size considered was 10 mL. Unfortunately, in many situations (for example, when testing developmental drugs or when characterizing explosives), even this limited sample size can be prohibitive.

The bulk density of a material, and its change under various standard test conditions, is commonly used to determine a material's flow behavior and to improve solids processing understanding. The bulk density of a material has been used to characterize the flowability of granular materials and powders.[22,23] There have been multiple studies comparing the bulk density to other flow characteristics.[24–28] Surface modification of powders often employs the bulk density as a quantitative assessment for the resulting improvement in the flow.[29,30] The bulk density has also been used to improve the understanding of several solids processing unit operations spanning industries: axial mixing,[31] granulation,[32–34] capsule filling,[35] fluidization,[36] food powder mixing,[37] and laser sintering of polymer parts.[38]

The bulk density is defined as the ratio of the mass of powder sample to the volume of that powder sample:

$$\rho_b = \frac{m_{sample}}{v_{sample}}$$

where ρ_b is the bulk density, m_{sample} is the mass of the sample, and v_{sample} is the volume of the sample. By definition, the bulk density accounts for the true density of the particles (through the mass term) and the interstitial space between the particles (through the volume term).[1] A useful derived quantity, the relative bulk density (also known as solids fraction), is readily defined as the ratio of the bulk density to the true density. A low relative bulk density is observed when a given mass of particles occupies a relatively large volume; typically observed in cohesive, poorly flowing materials. Counterintuitively, the high inter-particle forces, relative to gravity, prevent the particles from achieving a close packing arrangement.

Correspondence concerning this article should be addressed to B. J. Glasser at bglasser@rutgers.edu.

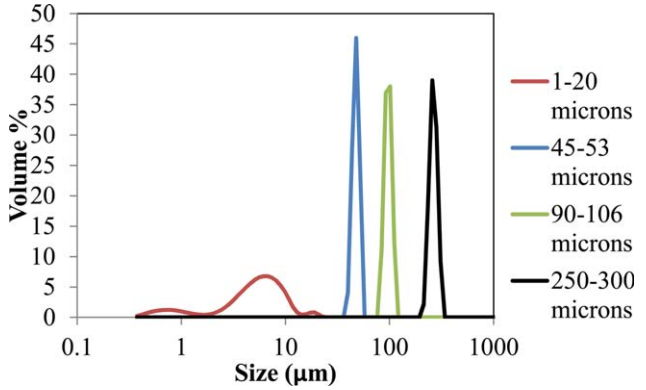

Figure 1. Particle-size distribution of glass beads, d_{50} in microns listed in legend.

[Color figure can be viewed in the online issue, which is available at wileyonlinelibrary.com.]

Alternatively, a high relative bulk density is observed when a given mass of particles occupies a relatively small volume, typically observed in free-flowing materials. The low interparticle forces, relative to gravity, results in closer packing.

For a given material, the bulk density (whether absolute or relative) is not a constant and is greatly dependent on the packing, or consolidation, state of the material.[39,40] During solids manufacturing, granular materials and powders undergo processing in a variety of environments. Due to their sensitivity to processing conditions, bulk density measurements can be used to determine a material's flowability (i.e., manufacturability) and, therefore, the extent to which the material may dilate or consolidate during manufacturing.[22,41] Since the bulk density measurement is highly dependent on the consolidation state of the material, the bulk density is typically considered at multiple packing states. Common measurement methods include: comparing the tapped and aerated states, such as the Carr Index and Hausner ratio[42,43]; comparing the density over a range of packing states, such as with the FT4 compressibility test[44]; and comparing the tapped and dilated states, such as with the GDR dilation test.[45]

This article introduces a new method for measuring the bulk flow behaviors of cohesive and noncohesive granular materials and powders using less than 50 mg of material (for the materials studied here). The solids fractions over a range of packing states are considered for 12 model systems with a wide range of flow properties. The rest of the article is organized as follows. The materials characterized and the experimental method used to measure the solids fractions are described in section "Materials and Methods." The effects of particle size and cohesion via capillary forces on the packing behavior are identified and discussed in section "Results," followed by conclusions in section "Conclusions."

Materials and Methods

Materials

A set of precision grade soda-lime glass beads (Mo-Sci Specialty Products, Rolla, MO) with four nonoverlapping particle-size distributions were used to study packing of granular systems in a small geometry. The four grades of glass beads had mean particle sizes of 5, 50, 100, and 275 microns (Figure 1). To remove any moisture acquired during storage, the glass beads were dried at 100°C for 1 h. While the dry 5 micron glass beads were observed to exhibit cohesive behaviors, the larger glass beads were observed to be relatively free-flowing. Attractive forces between particles were increased via the introduction of capillary forces. De-ionized water was added at 10% and 20% by weight. Taking into account the void space, 10% by weight corresponds to 12, 10, 9, and 5% by volume for 275, 100, 50, and 5 microns, respectively, and 20% by weight corresponds to 36, 35, 35, and 15% by volume for 275, 100, 50, and 5 microns, respectively, as shown in Table 1.

Table 1. Liquid Added by Volume Percent as a Function of Particle Size and Liquid Added by Mass Percent

	275 microns	100 microns	50 microns	5 microns
10% by mass	12%	10%	9%	5%
20% by mass	36%	35%	35%	15%

Methods

The solids fraction as a function of applied normal stress of the 12 model systems (four particle sizes at three moisture contents) was measured using a cup and piston design (Figure 2). A TA Instruments ARES RDA-III rheometer was used with custom plates (the cup and piston shown in Figure 2). The cup was cylindrical, 5 mm in diameter, and 1.5 mm in depth, and the piston was 5 mm in diameter and 5 mm in length. Material was poured into the cup until the cup was overfilled. The excess material was then scraped away. The mass of the remaining material in the cup was then measured. The sample mass was dependent on the initial bulk density of the material, but was typically less than 50 mg. The piston was subsequently lowered into the powder bed at a constant rate of 0.005 mm/s until the applied normal stress reached 1100 kPa, corresponding to a normal force of 21 N. The force imparted to the piston due to interaction with the cup wall spanned from 0.0 to 2.3 N and averaged 1.1 N with a standard deviation of 0.3 N, determined by measuring the force imparted to the piston when lowered into an empty cup. As a function of time, the bed height and normal force acting on the piston were recorded; sample data for the 275 micron particles is shown in Figure 3. The bed height decreases linearly with time, as expected. The force required to lower the piston was initially low and then, at a critical point, sharply increased. The horizontal separation of the data is due to variation in the time at which the piston first encountered the powder bed, i.e., the initial height of the powder bed. The largest variation observed in the data shown in Figure 3 is 124 microns, less than the average diameter of the particles. Thus, the difference in the powder bed height is less than one layer of particles. From this data, the solids fraction as a function of applied normal stress was calculated.

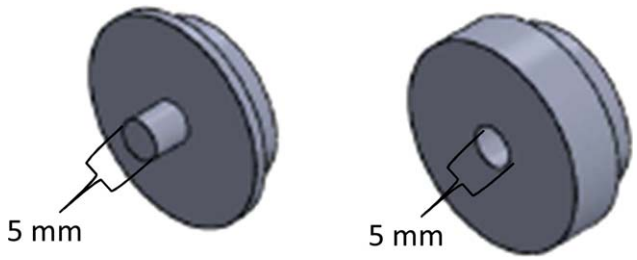

Figure 2. Schematics of cup and piston.

[Color figure can be viewed in the online issue, which is available at wileyonlinelibrary.com.]

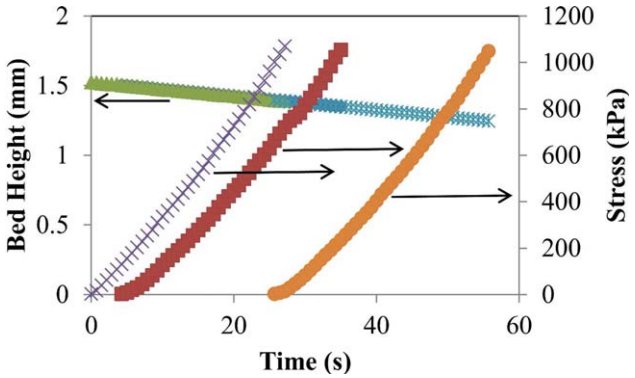

Figure 3. Example of data gathered using the small scale compressibility method; three repetitions for 275 micron glass beads are shown.

[Color figure can be viewed in the online issue, which is available at wileyonlinelibrary.com.]

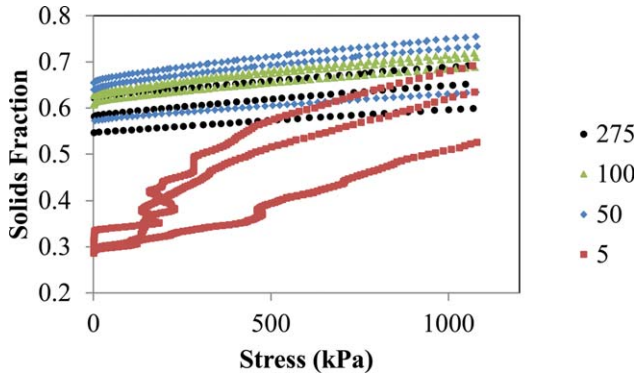

Figure 5. Effect of particle size on measured compressibility profiles; d_{50} in microns listed in legend.

[Color figure can be viewed in the online issue, which is available at wileyonlinelibrary.com.]

Results

An example of the measured solids fraction profiles for free-flowing conditions is depicted in Figure 4. Specifically, three repetitions of the 275 micron beads with 0% added moisture are shown. It was observed that the beads have an initial packing state with a porosity dependent on the cohesion of the material. As the normal force was applied, the beads rearranged to a position that could support a larger normal force. That is, the solids fraction increased with increasing applied normal force. The initial state was also dependent on the loading of the material into the cup. This potential source of variability could be mitigated by exercising care on the part of the user while loading the material. In addition to the initial variability, during each repetition, material rearrangement and consolidation occurred in a slightly different manner. As such, each repetition was considered as an individual event, instead of just considering their average, to preserve the information from each consolidation path.

Effect of particle size

The effect of particle size on the solids fraction profiles measured in the small geometry was determined. The glass beads with zero added liquid were characterized; the results are shown in Figure 5. It is known that as particle size decreases, cohesion due to van der Waals forces increases.[46] As a result, smaller particles tend to have lower bulk densities and have poorer flow properties. The general shape and magnitude of profiles for the three largest sizes studied here (50, 100, and 275 microns) are similar to one another. At low stress, the solids fraction varied from 0.55 to 0.65 and rose to 0.6 to 0.75 at higher stresses. The profiles are relatively flat and smooth, and as such, the solids fraction is not a strong function of the applied normal stress. These features of the profiles are indicative of freely flowing powders with low to zero cohesion.

However, as observed from Figure 5, the profiles of the 5 micron beads are markedly different from the other beads. At low applied normal stress, the solids fraction varies from 0.3 to 0.35, less than that of the larger particle sizes, and rises to 0.5 to 0.7 at higher stresses, similar to that of the larger particle sizes. The 5 micron profiles reflect a larger change in solids fraction with an increase in applied normal stress. In addition, these profiles are less smooth. These aspects are indicative of a cohesive material.

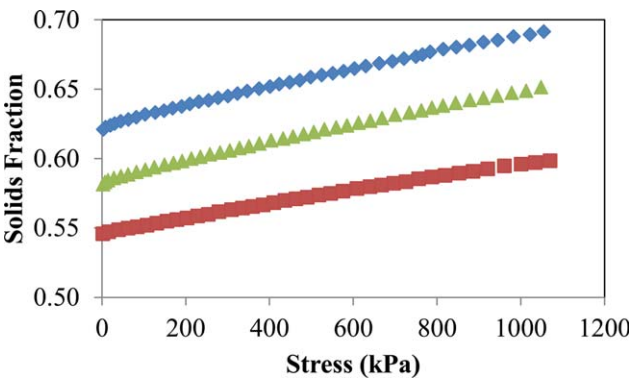

Figure 4. Example of compressibility profiles, three repetitions of 275 micron glass beads are shown.

[Color figure can be viewed in the online issue, which is available at wileyonlinelibrary.com.]

Effect of capillary forces

As previously discussed, to alter the cohesive forces between beads without changing the particle size, water was added to the glass beads in amounts corresponding to 10% and 20% by weight. The addition of liquid to the system introduced capillary forces between the beads. The solids fraction profiles for each particle size (275, 100, 50, and 5 microns) at each moisture content (0%, 10%, 20% by weight) are shown in Figure 6. Three repetitions are shown for each particle size at each moisture content. The profiles corresponding to the 275 micron beads (Figure 6A) show a reduction in solids fraction on the addition of 10% water and a subsequent increase in solids fraction on the addition of 20% water. The moisture content at 10% is sufficient to create liquid bridges between particles. This increase in attractive force manifests itself as an increase in cohesion and results in a more loosely packed powder. However, at 20% moisture, the amount of liquid in the system is enough to create a very viscous slurry. The amount of water between glass beads at this point is sufficient to entirely coat the particles. The layer of water lubricates the interaction between the beads, the result being an observed decrease in cohesion and an increase in the packing density of the material. The magnitude of the attractive forces between

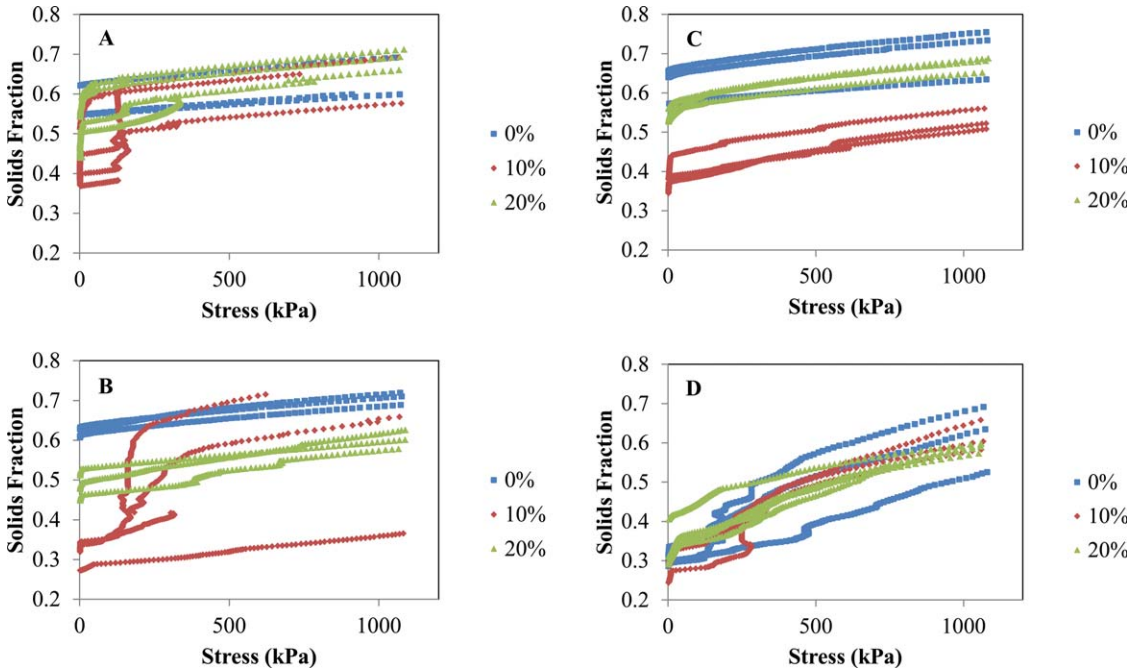

Figure 6. Effect of moisture content on (A) 275, (B) 100, (C) 50, and (D) 5 micron beads.

[Color figure can be viewed in the online issue, which is available at wileyonlinelibrary.com.]

the glass beads goes through a maximum at some point between 10% and 20% liquid added. Similar behavior was observed for the 100 (Figure 6B) and 50 micron (Figure 6C) particle sizes at each water content level.

The profiles for the 5 micron glass beads are shown in Figure 6D. The addition of water had a lesser impact on their packing behavior. This is likely largely due to the difference in surface area coverage between the particle sizes. The surface area to volume ratio of the 5 micron beads is much larger (at least one order of magnitude larger), therefore the same amount of water added by weight results in less coverage. In the small geometry studied here, it was observed that for the glass beads 50 microns in diameter and larger the cohesion increases with the addition of 10% water and subsequently decreases with the addition of 20% water. Once again, the 5 micron glass beads exhibited markedly different behavior.

Additional observations

In addition to the effects of particle size and capillary forces, two other observations were made regarding the solids fraction profiles. The first was that the consolidation occurred in two distinct regimes. The second observation was that the consolidation was not always smooth. These observations are discussed in greater detail below.

The Heckel equation is often used to describe compaction profiles of granular materials and powders, for example, those that describe tabletting processes[47]:

$$\ln\left(\frac{1}{1-\frac{V_s}{V}}\right) = KP + A$$

where V_s/V is the solids fraction, P is the applied normal stress, and K and A are fitted parameters. The left hand side of the Heckel equation is graphed along the y-axis and the stress is graphed along the x-axis (Figure 7). As a result, the solids fraction profiles are linear in the range that is described by the Heckel equation. A linear fit to the profile yields values for the parameters K and A as the slope and y-intercept, respectively. The y-intercept (A) reflects the porosity (including liquid volume fraction in the cases where liquid is present) at zero applied normal stress, e.g., the conditions during die filling and particle rearrangement before deformation of the particles occurs. The slope (K) reflects the reduction in porosity (including liquid volume fraction in the cases where liquid is present) as a function of applied normal stress. It was found that past a critical packing state, the Heckel equation fit the solids fraction profiles measured here reasonably well. The profiles corresponding to the 275 micron glass beads with 0% added moisture are shown in Figure 7 with I, II, and III each denoting a repetition. For this material, the critical packing state where the Heckel equation begins to describe the consolidation

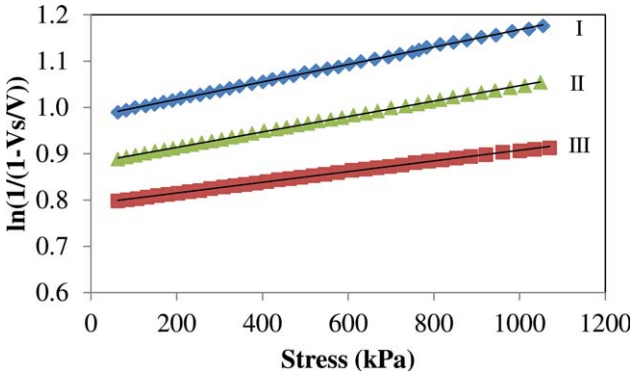

Figure 7. Example of fitting Heckel equation to the compressibility profiles at stresses larger than 50 kPa, 275 micron at 0% added water shown.

The regression statistics for the fits are as follows: (I) $R^2 = 0.9995$ with P-value <0.001, (II) $R^2 = 0.0006$ with P-value < 0.001, and (III) $R^2 = 0.9992$ with P-value < 0.001. [Color figure can be viewed in the online issue, which is available at wileyonlinelibrary.com.]

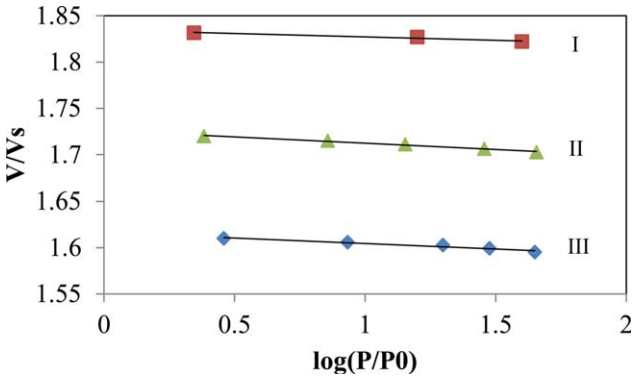

Figure 8. Example of fitting Walker equation to the compressibility profiles at low stresses (less than 50 kPa), 275 micron at 0% added water shown.

The regression statistics for the fits are as follows: (I) $R^2 = 0.9582$ with P-value $=0.005$, (II) $R^2 = 0.9850$ with P-value $= 0.001$, and (III) $R^2 = 0.9494$ with P-value $= 0.131$. [Color figure can be viewed in the online issue, which is available at wileyonlinelibrary.com.]

behavior occurs at around 50 kPa. A linear fit to the profile labeled as "I" has a slope (K) of 0.0002 and a y-intercept (A) of 0.9361 with a coefficient of determination (R^2) of 0.9995 and a P-value less than 0.001. Similar observations were made for each of the 12 model systems studied here.

However, in the low stress range, the Heckel equation does not describe the consolidation behavior. This has been observed previously in the literature. It was found that prior to the critical packing state at which the Heckel equation begins to describe the consolidation behavior, there exists a first regime of consolidation behavior. For this first regime at low stresses, the Walker equation fit the solids fraction profiles measured here reasonably well. The Walker equation, although used less frequently to describe compaction profiles, could be used to describe behavior at low stresses in our experiments[47]:

$$\frac{V}{V_s} = a - K\ln\left(\frac{P}{P_0}\right)$$

where V_s/V is the solids fraction, P/P_0 is the stress normalized by the unit stress, and a and K are fitted parameters. The inverse of the solids fraction was graphed as a function of the natural log of the stress normalized by a reference stress. As a result, the solids fraction profiles are linear in the range that is described by the Walker equation. A linear fit to the profile yields values for the parameters K and a as the slope and y-intercept, respectively. The y-intercept is the measured solids fraction at an applied normal stress of 1 kPa (the reference applied normal stress). The slope describes the curvature of the solids fraction profile.

The profiles corresponding to the 275 micron glass beads with 0% added moisture are shown in Figure 8 with I, II, and III each denoting a repetition. The maximum stress considered here is 50 kPa as this was identified as the critical transition point between the Heckel and Walker equations for this material. A linear fit to the profile labeled as "II" has a slope (K) of -0.0204 and a y-intercept (a) of 1.7412 with a coefficient of determination (R^2) of 0.985 and a P-value of 0.001. Similar observations were made for each of the 12 model systems studied here. The average value for the slope and y-intercept parameters from the Walker equation fit to each of the 12 model systems is shown in Figure 9. The value of a denotes the y-intercept of the Walker equation and represents the solids fraction at a reference applied normal stress of P_0, taken to be 1 kPa here. The value of a for 0% moisture content was similar for the 275, 100, and 50 micron beads; thus they each approach a similar solids fraction at the reference applied normal stress. This would be expected since they are all fairly mono-dispersed glass particles that are roughly spherical and noncohesive.

The a-value for the 5 micron beads at 0% moisture content is much larger and different from the three other particle sizes. Again, this would be expected since the 5 micron particles are cohesive and it would then be expected that they would reach a lower solids fraction than the noncohesive beads at the same reference applied normal stress.

The value of K describes the curvature of the solids fraction profile. The value of K for 0% moisture content is similar and small in magnitude for the 275, 100, and 50 micron beads; thus the profiles each have a similarly flat shape, i.e., the solids fraction is relatively independent of applied normal stress. Again, this would be expected since the particles are fairly mono-dispersed, spherical, and noncohesive. The K-value for the 5 micron beads at 0% moisture content is much larger and different from the three other particle sizes. Again, this would be expected since the 5 microns particles are cohesive and it would be expected that the solids fraction would increase as a function of applied normal stress.

Revisiting the a-values (y-intercepts), the addition of 10% liquid led to a relatively large increase in a-value, of similar magnitudes for the 275, 100, and 50 micron particles. This is

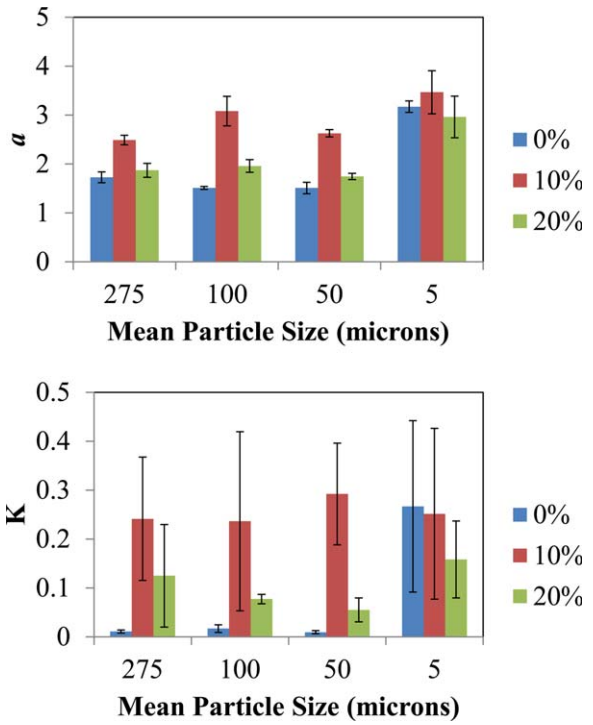

Figure 9. Parameter fits of the Walker equation (y-intercept, top; slope, bottom) to measured compressibility profiles up to 50 kPa.

[Color figure can be viewed in the online issue, which is available at wileyonlinelibrary.com.]

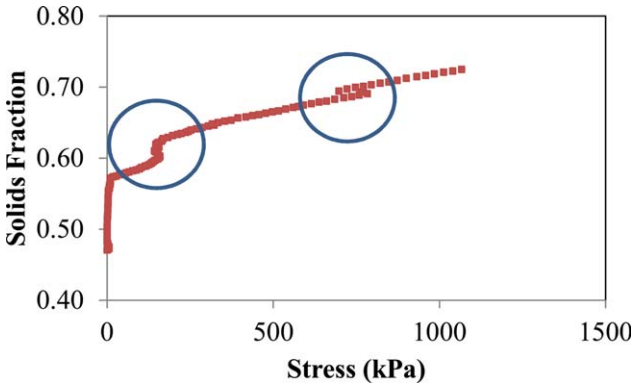

Figure 10. Example of horizontal features in a measured profile of 100 micron beads with 20% added moisture.

[Color figure can be viewed in the online issue, which is available at wileyonlinelibrary.com.]

to be expected since the addition of liquid increases the cohesion of the system and leads to a lower solids fraction at the reference applied normal stress (the Walker equation is inversely proportional to the solids fraction). The addition of 10% liquid to the 5 micron particles also led to an increase in *a*-value, but the increase was smaller in magnitude. As discussed previously, this may be due to the difference in surface area between the particle sizes. The 5 micron particles have a much larger (at least one order of magnitude larger) surface area to volume ratio and as a result the same amount of liquid added by mass results in lower surface area coverage (or much thinner coverage). From Figure 9, it is observed that adding 20% liquid by mass results in a decrease in cohesion of similar magnitudes for the 275, 100, and 50 micron particles, as addition of 20% liquid created a very viscous slurry. The surface coverage of the water was sufficient to lubricate the particles increasing the packing density of the particles. The addition of 20% liquid to the 5 micron particles also led to a decrease in *a*-value, but the decrease was smaller in magnitude; again potentially due the difference in surface area coverage between the particle sizes. As observed from Figure 9, the effect of the moisture content on the slope parameter of the Walker equation (the value of *K*) was similar to that observed for the *y*-intercept (the value of *a*).

It was observed that the effect of the moisture content was more clearly visible than the effect of the particle size on the slope (*K*) and *y*-intercept (*a*). The error of the parameter fits was calculated as the standard deviation of the results of the three repetitions for each material. The error of the slope fit (Figure 9, bottom) was much higher than the *y*-intercept fit (Figure 9, top). There was a certain amount of error in filling the small geometry with cohesive beads; the main source in the variability of the solids fraction at 1 kPa, the reference applied normal stress. Additionally, the path of consolidation was highly variable, especially in the initial states. As a result, the shape of the solids fraction profile—characterized by the slope of the Walker equation—was highly variable, indicated by the large error bars of the slope measurement.

The second additional observation was that the consolidation was not always smooth. In fact, horizontal features appeared in several of the measured solids fraction profiles. An example of these features occurring in a solids fraction profile measured for the 100 micron beads with 20% by weight added moisture is depicted in Figure 10. In some instances, the stress on the piston would suddenly decrease, and to a larger extent than would be expected from stick/slip of the piston on the cup walls as discussed in section "Materials and Methods." These events are consistent with what has been described in the literature as "snap-through buckling."[48] As the piston descended into the powder bed, meta-stable structures (rings, arches, etc.) could form within the bed that are able to withstand a certain level of load. Once the force applied to the structure exceeds the resistance of the metastable structures, the metastable structures would break, and a sudden "catastrophic" event would be triggered, where the bed would experience a dramatic repacking and reduction in void space. The size and frequency of these events may be dependent on how easily the structures form and how strong the structures are once formed. This may be related to the material's cohesion. The size and frequency of these events have also been observed to be highly variable, so a large number of experiments and/or simulations would be required to obtain statistically representative results.

Validation of the characterization method

The solids fraction profiles (shown in Figure 6) and parameters from the Walker equation (shown in Figure 9) follow trends previously observed for bulk materials. One might expect the cohesion of the system to increase due to van der Waals forces as the particle size decreases. This is, in fact, what was observed. The increase in cohesion in the 5 micron beads resulted in lower packing fractions and a steeper solids fraction profile. It has been previously shown in the literature that the addition of moisture into a powder, with the formation of capillary "necks," initially increases the cohesion in the system and lowers the observed packing fractions. As the moisture content increases further, the particles become lubricated resulting in an increase in the packing fraction. This effect was also observed here, in the small geometry. The general behavior that one might expect to observe based on experience and behavior known at larger scales is in fact also observed in the small geometry used here.

The solids fraction profiles measured in the small geometry were validated against a solids fraction profile measurement at a larger scale, using the compressibility test, obtained using the FT4 from Freeman Technology. The 10 mL cell (with a

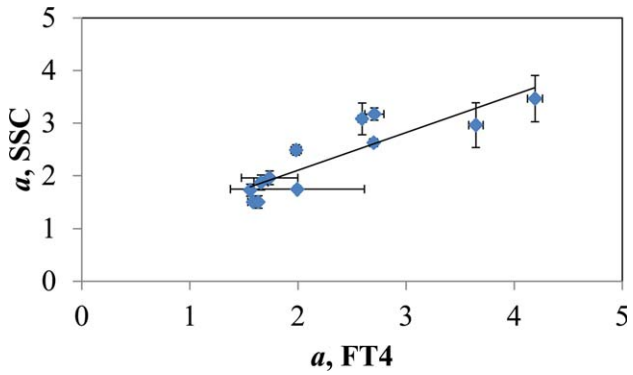

Figure 11. Y-intercept from Walker equation fit of small scale compressibility and FT4 for each material.

The regression equation was $y = 0.7164x + 0.6706$ and had an R^2 of 0.771 and *P*-value less than 0.001. [Color figure can be viewed in the online issue, which is available at wileyonlinelibrary.com.]

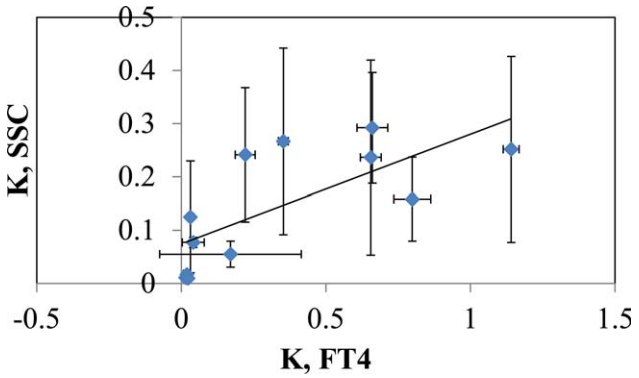

Figure 12. Slope from Walker equation fit of small scale compressibility and FT4.

The regression equation was $y = 0.2055x + 0.0742$ and had an R^2 of 0.511 and a P-value of 0.009. [Color figure can be viewed in the online issue, which is available at wileyonlinelibrary.com.]

diameter of 25 mm) was used to measure the compressibility of each of the 12 model systems in the FT4. Because a conditioning step was not used at the small scale, the conditioning step was also not used during the FT4 testing. Of note, the compressibility test carried out using the FT4 had a maximum applied normal stress of 15 kPa; two orders of magnitude less than with the small scale system.

It might be expected that the FT4 system would not capture all the relevant behavior occurring at the small scale. The effect of the container walls on the force needed to consolidate the material, and to some extent the structure of the repackaged material, is much more significant at the small scale as a larger portion of the particles in the system interact with the boundary of the geometry. Additionally, by nature of the small scale, the breaking of the formed meta-stable structures within the bed could be resolved. At larger scales, these events are smaller compared to the size of the system, also occur more frequently, and thus their effect is averaged. Single events are less likely to be resolved.

Nonetheless, for the sake of comparison, the Walker equation was fit to the profiles measured using the FT4 and the slope and y-intercept parameters were extracted. The Walker equation was used for the comparison to the FT4 as this equation exhibits better fits at low stresses. Overall, there was good qualitative agreement between methods. The values for the parameters measured by each system was compared using parity plots (Figures 11 and 12). The linear regression obtained between the y-intercept parameter values from each system had a regression equation of $y = 0.7164x + 0.6706$ with a coefficient of determination of 0.77 and P-value less than 0.001 (Figure 11). It was observed that the error in the measurement of the y-intercept, a, (calculated as the standard deviation of three measurements and depicted as error bars) using the FT4 and the small scale system were similar. The linear regression obtained between the slope parameter values from each system had a regression equation of $y = 0.2055x + 0.0742$ with a coefficient of determination of 0.51 and P-value of 0.009 (Figure 12). It was observed that the error in the measurements of the slope, K, obtained using the small scale system were much larger than those obtained by the FT4. This was expected since, as previously discussed, the slope captures the curvature of the solids fraction profile and this was highly variable. The coefficient of determination values represent the amount of explained variance. These results can be interpreted as 77% and 51% of the variability in the y-intercept and slope, respectively, measured at the small scale was also observed at the larger scale. These values indicate that the FT4 captured a statistically significant portion of the behavior occurring during the consolidation at the small scale. The statistical significance of the correlations between measurements obtained from the two devices is actually quite high, as indicated by the very low values of P (the probability that the observed correlation is just due to random alignment of the data). The relatively low values of R are simply due to the fact that the large scale device only captures a fraction of the behavior observed in the small device; the remainder of the variance was likely due to the wall effects and catastrophic repacking, neither of which should be significant in the large scale device.

Conclusions

This article demonstrates that the packing state of cohesive model systems as a function of applied normal stress, which can be considered as a bulk flow property, can be measured using less than 50 mg of material. This is an important development and could have applications in situations where the amount of material available for testing is restricted. The solids fraction profiles of 12 model systems with a range of flow properties were measured. It was found that the packing fractions decreased with decreasing particle diameters. It was also found that the effect of moisture addition initially increases the cohesive forces between particles due to capillary forces, but as the moisture content increases the moisture lubricates the particles and results in an increase in the packing fraction. These observations are consistent with expectations derived from the behavior of these materials at a larger scale.

Consolidation of the materials occurred in two regimes: the Walker equation describes the packing behavior at very low stresses and the Heckel equation describes the packing behavior at higher stresses. During consolidation, metastable structures were formed and then broken within the powder bed. Due to the resolution of the small scale system, such collapses in the powder bed were resolved. The measurements obtained at the small scale were validated against known and expected behavior as well as against a traditional method, the Freeman Technology FT4 compressibility test. Additional effects, such as the wall effects and the collapsing events were captured by the small scale system. For the behavior captured by both systems, good qualitative correlation between the small scale system and traditional measurement was observed.

The results presented here are based on a limited number of repetitions. Further work, i.e., additional repetitions through simulations and/or extensive experimentation, is needed to describe and characterize the breaking of the meta-stable structures formed during packing in a statistically meaningful manner. Additionally, work using other materials with broader particle-size distributions would be of interest.

Acknowledgments

The authors would like to acknowledge financial support from DOD-ARMY-ACC-W15QKN-11-C-0118.

Literature Cited

1. Rhodes M. *Introduction to Particle Technology, 2nd ed.* West Sussex, UK: Wiley, 2008.

2. Shinbrot T, LaMarche K, Glasser BJ. Triboelectrification and razorbacks: geophysical patterns produced in dry grains. *Phys Rev Lett.* 2006;96(17):178002.
3. Geldart D. Powder processing – the overall view. In: Rhodes MJ, editor. *Principles of Powder Technology*, *1st ed.* New York: Wiley; 1991:1–7.
4. Bates L. The need for industrial education in bulk technology. *Bulk Solids Handl.* 2006;26(7):464–475.
5. Bridgewater J. The dynamics of granular materials – towards grasping the fundamentals. *Granular Matter.* 2003;4(4):175–181.
6. Ennis BJ, Green J, Davies R. Particle technology – the legacy of neglect in the U.S. *Chem Eng Prog.* 1994;90:32–43.
7. MiDi GDR. On dense granular flows. *Eur Phys J E.* 2004;14(4): 341–365.
8. Rietema K. Powders, what are they? *Powder Technol.* 1984;37(1): 5–23.
9. Schwedes J. Review on testers for measuring flow properties of bulk solids. *Granular Matter.* 2003;5(1):1–43.
10. Galarraga C, Peluso E, de Lasa H. Eggshell catalysts for Fischer-Tropsch synthesis: modeling catalyst impregnation. *Chem Eng J.* 2001;82(1–3):13–20.
11. Liu X, Khinast JG, Glasser BJ. A parametric investigation of impregnation and drying of supported catalysts. *Chem Eng Sci.* 2008;63:4517–4530.
12. Poux M, Fayolle P, Bertrand J, Bridoux D, Bousquet J. Powder mixing: some practical rules applied to agitated systems. *Powder Technol.* 1991;68(3):213–234.
13. Muzzio FJ, Alexander A, Goodridge C, Shen E, Shinbrot T. Solids mixing. In: Paul EL, Atiemo Obeng VA, Kresta S, editors. *Handbook of Industrial Mixing*. New York: Wiley, 2004:887–985.
14. Radl S, Kalvoda E, Glasser BJ, Khinast JG. Mixing characteristics of wet granular matter in a bladed mixer. *Powder Technol.* 2010; 200(3):171–189.
15. Remy B, Glasser BJ, Khinast JG. The effect of mixer properties and fill level on granular flow in a bladed mixer. *AIChE J.* 2010;56(2): 336–353.
16. Lamberto DJ, Cohen B, Marencic J, Miranda C, Petrova R, Sierra L. Laboratory methods for assessing API sensitivity to mechanical stress during agitated drying. *Chem Eng Sci.* 2011;66(17):3868–3875.
17. Hare C, Ghadiri M, Dennehy R. Prediction of attrition in agitated particle beds. *Chem Eng Sci.* 2011;66(20):4757–4770.
18. Liu LX, Marziano I, Bentham AC, Litster JD, White ET, Howes T. Effect of particle properties on the flowability of ibuprofen powders. *Int J Pharm.* 2008;362(1–2):109–117.
19. Hare CL, Ghadiri M. Influence of measurement cell size on predicted attrition by the distinct element method. *Powder Technol.* 2013;236:100–106.
20. Koynov S, Glasser B, Muzzio F. Comparison of three rotational shear cell testers: powder flowability and bulk density. *Powder Technol.* 2015;283:103–112.
21. Hughes H, Leane MM, Tobyn M, Gamble JF, Munoz S, Musembi P. Development of a material sparing bulk density test comparable to a standard USP method for use in early development of API's. *AAPS PharmSciTech.* 2015;16:165–170.
22. Abdullah EC, Geldart D. The use of bulk density measurements as flowability indicators. *Powder Technol.* 1999;102(2):151–165.
23. Chi-Ying Wong A. Characterisation of the flowability of glass beads by bulk densities ratio. *Chem Eng Sci.* 2000;55(18):3855–3859.
24. Leturia M, Benali M, Lagarde S, Ronga I, Saleh K. Characterization of flow properties of cohesive powders: a comparative study of traditional and new testing methods. *Powder Technol.* 2014;253:406–423.
25. Kojima T, Elliott JA. Incipient flow properties of two-component fine powder systems and their relationships with bulk density and particle contacts. *Powder Technol.* 2012;228:359–370.
26. Saw HY, Davies CE, Jones JR, Paterson AHJ. Shear testing of lactose powders: the influence of consolidation stress and particle size on bulk density and estimated cohesion. *Adv Powder Technol.* 2014; 25(4):1164–1170.
27. Stanley-Wood N, Sarrafi M, Mavere Z, Schaefer M. The relationships between powder flowability, particle re-arrangement, bulk density and Jenike failure function. *Adv Powder Technol.* 1993;4(1):33–40.
28. Vasilenko A, Glasser BJ, Muzzio FJ. Shear and flow behavior of pharmaceutical blends – method comparison study. *Powder Technol.* 2011;208(3):628–636.
29. Mullarney MP, Beach LE, Davé RN, Langdon BA, Polizzi M, Blackwood DO. Applying dry powder coatings to pharmaceutical powders using a comil for improving powder flow and bulk density. *Powder Technol.* 2011;212(3):397–402.
30. Jallo LJ, Ghoroi C, Gurumurthy L, Patel U, Davé RN. Improvement of flow and bulk density of pharmaceutical powders using surface modification. *Int J Pharm.* 2012;423(2):213–225.
31. Tallon S, Davies CE. In-situ monitoring of axial particle mixing in a rotating drum using bulk density measurements. *Powder Technol.* 2008;186(1):22–30.
32. Zuurman K, Bolhuis GK, Vromans H. Effect of binder on the relationship between bulk density and compactibility of lactose granulations. *Int J Pharm.* 1995;119(1):65–69.
33. Zuurman K, Riepma KA, Bolhuis GK, Vromans H, Lerk CF. The relationship between bulk density and compactibility of lactose granulations. *Int J Pharm.* 1994;102(1–3):1–9.
34. Hapgood KP, Litster JD, Biggs SR, Howes T. Drop penetration into porous powder beds. *J Colloid Interface Sci.* 2002;253(2):353–366.
35. Faulhammer E, Llusa M, Radeke C, Scheibelhofer O, Lawrence S, Biserni S, Calzolari V, Khinast JG. The effects of material attributes on capsule fill weight and weight variability in dosator nozzle machines. *Int J Pharm.* 2014;471(1–2):332–338.
36. Wong AC-Y. Use of angle of repose and bulk densities for powder characterization and the prediction of minimum fluidization and minimum bubbling velocities. *Chem Eng Sci.* 2002;57(14):2635–2640.
37. Shenoy P, Viau M, Tammel K, Innings F, Fitzpatrick J, Ahrné L. Effect of powder densities, particle size and shape on mixture quality of binary food powder mixtures. *Powder Technol.* 2015;272:165–172.
38. Ziegelmeier S, Christou P, Wöllecke F, Tuck C, Goodridge R, Hague R, Krampe E, Wintermantel E. An experimental study into the effects of bulk and flow behaviour of laser sintering polymer powders on resulting part properties. *J Mater Process Technol.* 2015;215:239–250.
39. Vasilenko A, Koynov S, Glasser BJ, Muzzio FJ. Role of consolidation state in the measurement of bulk density and cohesion. *Powder Technol.* 2013;239:366–373.
40. Ford KJ, Gilchrist JF, Caram HS. Transitions to vibro-fluidization in a deep granular bed. *Powder Technol.* 2009;192(1):33–39.
41. Grey RO, Beddow JK. On the Hausner Ratio and its relationship to some properties of metal powders. *Powder Technol.* 1969;2(6):323–326.
42. Carr RL. Evaluating flow properties of solids. *Chem Eng.* 1965;72: 163–168.
43. Hausner H. Friction conditions in a massive metal powder. *Int J Powder Metal.* 1967;4:7.
44. Freeman R. Measuring the flow properties of consolidated, conditioned and aerated powders — A comparative study using a powder rheometer and a rotational shear cell. *Powder Technol.* 2007;174:25–33.
45. Faqih A, Chaudhuri B, Muzzio FJ, Tomassone MS, Alexander A, Hammond S. Flow – induced dilation of cohesive granular materials. *AIChE J.* 2006;52(12):4124–4132.
46. Schulze D. *Powders and Bulk Solids: Behavior, Characterization, Storage and Flow*. Berlin: Springer-Verlag, 2008.
47. Sonnergaard JM. A critical evaluation of the Heckel equation. *Int J Pharm.* 1999;193(1):63–71.
48. Gioia G, Cuitiño AM, Zheng S, Uribe T. Two-phase densification of cohesive granular aggregates. *Phys Rev Lett.* 2002;88(20):204302.

Manuscript received June 16, 2015, and revision received Nov. 28, 2015.